

# How Transformers Reject Wrong Answers: Rotational Dynamics of Factual Constraint Processing

Javier Marín  
www.cert-framework.com  
*javier@jmarin.info*

February 2026

## Abstract

When a language model is fed a wrong answer, what happens inside the network? Current understanding treats truthfulness as a static property of individual-layer representations—a direction to be probed, a feature to be extracted. Less is known about the dynamics: how internal representations diverge across the full depth of the network when the model processes correct versus incorrect continuations.

We introduce forced-completion probing, a method that presents identical queries with known correct and incorrect single-token continuations and tracks five geometric measurements across every layer of four decoder-only models (1.5B–13B parameters). We report three findings. First, correct and incorrect paths diverge through rotation, not rescaling: displacement vectors maintain near-identical magnitudes while their angular separation increases, meaning factual selection is encoded in direction on an approximate hypersphere. Second, the model does not passively fail on incorrect input—it actively suppresses the correct answer, driving internal probability away from the right token. Third, both phenomena are entirely absent below a parameter threshold and emerge at 1.6B, suggesting a phase transition in factual processing capability.

These results show that factual constraint processing has a specific geometric character—rotational, not scalar; active, not passive—that is invisible to methods based on single-layer probes or magnitude comparisons.

## 1 Introduction

Transformer language models generate fluent text that can be factually incorrect [Ji et al., 2023, Huang et al., 2023]. Understanding how these errors arise inside the model is a prerequisite for principled mitigation. A growing body of work has established that hidden representations encode linearly separable features related to truthfulness [Burns et al., 2023, Azaria and Mitchell, 2023, Li et al., 2023, Marks and Tegmark, 2023], that factual associations can be localized to specific layers and components [Meng et al., 2022, Geva et al., 2023], and that intermediate representations can be decoded into output distributions via the logit lens [nostalgebraist, 2020, Belrose et al., 2023]. Dai et al. [2022] identified individual ‘knowledge neurons’ in FFN layers whose activations are causally linked to specific facts.

However, these approaches characterize truthfulness as a static property of individual-layer representations like a direction in activation space [Marks and Tegmark, 2023] or a linear probe at a particular depth [Azaria and Mitchell, 2023]. They do not explain how the distinction between correct and incorrect processing emerges, evolves, and resolves across the full depth of the network.

This limits their utility for detection because a method built on a single-layer snapshot cannot exploit dynamics that unfold over many layers. Our method, forced-completion probing, builds queries with known correct and incorrect single-token continuations and measures five complementary quantities across every layer: trajectory similarity, displacement geometry, linear probe accuracy, logit lens commitment, and attention allocation. By forcing the model to process both answers of the same query, we obtain matched pairs that isolate the effect of factual correctness from confounds such as token frequency or syntactic complexity. In three models that show the phenomena (LLaMA-2 13B, Mistral 7B, StableLM-2 1.6B) and one that does not (Qwen2 1.5B), we find:

1. **Rotational divergence.** Correct and incorrect answer paths separate through angular rotation on an approximately constant-norm manifold, not through scaling. Displacement norm ratios remain within 3% of unity while cosine similarity drops to 0.62–0.69 at intermediate layers.
2. **Active suppression.** For incorrect answers, the logit lens commitment ratio does not only stagnate—it collapses to  $\kappa_{\min} = 0.08$  in the two larger models ( $p < 10^{-100}$ , one-sample  $t$ -test against  $\kappa = 0.5$ ), meaning the model actively drives probability away from the correct token.
3. **Scale threshold.** All five measurements are at chance in Qwen2 1.5B ( $n = 300$  queries). The phenomena emerge at 1.6B parameters (StableLM-2) and strengthen with scale, consistent with a phase transition in factual processing capability.

## 2 Related Work

### 2.1 Representation geometry

Park et al. [2024] formalized the linear representation hypothesis, showing that high-level concepts correspond to linear directions in transformer hidden states. Gurnee and Tegmark [2024] demonstrated that this structure extends to spatial and temporal coordinates, with individual neurons reliably encoding real-world quantities. Dar et al. [2023] showed that transformer computations can be interpreted directly in embedding space, and Hernandez et al. [2024] established that relational knowledge is decoded through linear transformations. Zou et al. [2023] demonstrated that this geometric structure can be exploited not only for analysis but for intervention, reading and controlling model behavior through directions in activation space. Ethayarajh [2019] showed that contextual representations are highly anisotropic, occupying a narrow cone rather than distributing uniformly—a constraint relevant to interpreting geometric claims about hidden-state manifolds. Collectively, these results establish that geometric analysis of hidden states reveals genuine computational structure—not artifacts of high dimensionality. Our contribution is to show that factual constraint processing produces a specific geometric signature—*isometric divergence*—that differentiates it from general representational structure.

### 2.2 Probing truthfulness in hidden states

Burns et al. [2023] showed that unsupervised methods can discover latent knowledge in language model representations. Azaria and Mitchell [2023] demonstrated that simple classifiers trained on hidden states predict whether a model’s output is true. Li et al. [2023] extended this to inference-time intervention, shifting activations along truthfulness directions. Marks and Tegmark [2023] characterized the geometry of truth as an emergent linear structure. These approaches establish that truthfulness is encoded in hidden states, but characterize it as a static property at individual

layers—they do not track how the distinction between correct and incorrect processing emerges and resolves across network depth.

### 2.3 Factual recall mechanisms

Meng et al. [2022] localized factual associations to mid-layer MLP modules. Geva et al. [2023] decomposed factual recall into attribute extraction and entity enrichment phases. Geva et al. [2021] showed that feed-forward layers function as key-value memories. This body of work establishes where factual processing occurs and which components are involved, but does not characterize the geometric dynamics of how correct and incorrect answers diverge during processing.

### 2.4 Logit lens and iterative inference

nostalgebraist [2020] introduced decoding intermediate representations through the unembedding matrix, enabling inspection of what a model “believes” at each layer. Belrose et al. [2023] refined this with the tuned lens, improving faithfulness of intermediate predictions. Din et al. [2023] studied when models reach their final answer early, establishing that commitment to an output can vary across depth. These tools make intermediate states readable but have not been used to define quantitative measures of how processing dynamics differ between correct and incorrect answers—the commitment ratios we introduce in Section 3.

## 3 Geometric Measurements

We measure five quantities across every layer of a transformer processing correct versus incorrect responses. Let  $h_\ell^q \in \mathbb{R}^d$  denote the hidden-state representation of the query alone at layer  $\ell$ , and  $h_\ell^+, h_\ell^- \in \mathbb{R}^d$  the representations when the correct or incorrect answer token is appended.

**(M1) Trajectory similarity.** The cosine similarity  $\tau(\ell) = \cos(h_\ell^+, h_\ell^-)$  measures how similar the hidden states for correct and incorrect answers are at layer  $\ell$ . When  $\tau$  is near unity, the model has not yet differentiated the two answers; when it drops, the representations have diverged.

**(M2) Displacement geometry.**

**Definition 1** (Displacement field). *The answer displacement at layer  $\ell$  is*

$$d_\ell^\pm = h_\ell^\pm - h_\ell^q \in \mathbb{R}^d. \tag{1}$$

*This vector captures how appending an answer token shifts the representation away from the query-only state.*

**Definition 2** (Rotational divergence). *The angular divergence between correct and incorrect answer paths is*

$$\rho(\ell) = 1 - \frac{\langle d_\ell^+, d_\ell^- \rangle}{\|d_\ell^+\| \cdot \|d_\ell^-\|}, \tag{2}$$

*and the norm ratio is  $\eta(\ell) = \|d_\ell^+\|/\|d_\ell^-\|$ .*

Together,  $\rho$  and  $\eta$  decompose the divergence between answer paths into angular and radial components. If the two paths separate primarily through direction change ( $\rho$  increases) while maintaining similar magnitudes ( $\eta \approx 1$ ), then factual selection is encoded in orientation on the hidden-state manifold, not in scale. We call this isometric divergence: the representations lie on an

approximate hypersphere, and factual selection corresponds to rotation on this manifold. This is the central geometric claim of the paper, tested empirically in Section 5.

**(M3) Linear probing.** A logistic regression classifier trained on hidden states at each layer to predict correct vs. incorrect answer. Probe accuracy measures how linearly separable the two classes are at each depth. Following Hewitt and Liang [2019], we use control tasks (our neutral query category; see Section 4) to assess probe selectivity. If probes achieve high accuracy on neutral queries where no factual constraint exists, they are detecting artifacts of the forced-completion setup rather than factual processing.

**(M4) Commitment ratio.**

**Definition 3** (Commitment ratio). *Let  $\phi : \mathbb{R}^d \rightarrow \mathbb{R}^{|V|}$  denote the unembedding projection. For token indices  $t^+$  (correct) and  $t^-$  (incorrect):*

$$\kappa(\ell) = \frac{\exp(\phi(h_\ell)[t^+])}{\exp(\phi(h_\ell)[t^+]) + \exp(\phi(h_\ell)[t^-])}. \quad (3)$$

*When processing the correct answer,  $\kappa(\ell)$  measures the model’s intermediate confidence in the correct token. When processing the incorrect answer,  $\kappa(\ell)$  measures whether the model’s internal state still favors the correct answer despite being forced to process the wrong one.*

**Definition 4** (Active suppression). *A model shows active suppression at layer  $\ell$  if, when processing the incorrect answer,  $\kappa(\ell) < 0.5 - \epsilon$  for significance threshold  $\epsilon > 0$ . This means the intermediate representation actively favors the incorrect token over the correct one—the model is not only uncertain but is driving probability away from the right answer. The suppression depth  $\sigma = 0.5 - \kappa_{\min}$  quantifies the strength of this effect.*

If factual processing involves active rejection rather than passive failure, we should observe  $\kappa(\ell) \ll 0.5$  at intermediate layers when models process incorrect answers. We test this prediction in Section 5.

**(M5) Attention allocation ratio.**

**Definition 5** (Attention allocation ratio). *For deep-constraint token set  $T_d$  and surface token set  $T_s$  at layer  $\ell$ :*

$$\alpha(\ell) = \frac{\sum_{t \in T_d} a_\ell(t)}{\sum_{t \in T_d} a_\ell(t) + \sum_{t \in T_s} a_\ell(t)} \quad (4)$$

*where  $a_\ell(t)$  is the attention weight on token  $t$ , averaged across heads.*

If the commitment collapse observed for incorrect answers has a mechanistic origin in attention patterns, correct answers should allocate systematically more attention to deep-constraint tokens:  $\alpha^+(\ell) > \alpha^-(\ell)$  across layers. We test this prediction in Section 5.

## 4 Experimental Setup

### 4.1 Experimental Dataset

We form queries designed to have exactly one correct single-token continuation. For example, “In the US, an ambulance responds to a medical emergency. Dial:” requires “911” (correct) versus “999” (incorrect, which is the UK number). Each query specifies a deep constraint—a factual requirement embedded in the question context—and the correct/incorrect tokens are chosen

to be semantically related but factually distinct. When we force a model to process “911” versus “999” after a US emergency query, something measurable happens inside the network. But we need to determine whether this happens because the model is performing factual reasoning—matching “US” to “911”—or whether the same dynamics arise whenever a model processes any right-versus-wrong answer, even a trivial one. Testing only hard factual queries cannot differentiate these cases. We therefore build three query categories that require progressively less factual knowledge to answer correctly:

1. **Deep constraint** (DC,  $n = 182$ ): The correct answer requires integrating a domain-specific factual rule with the query context—for example, matching a jurisdiction to its emergency number, a drug to its dosage limit, or a financial instrument to its regulatory threshold. The model must retrieve and apply a specific fact, not only follow syntactic or semantic cues.
2. **Control** (CTRL,  $n = 66$ ): The query has a single correct answer, but arriving at it requires less domain-specific reasoning—for example, completing a well-known sequence or identifying a commonly associated entity. These queries test whether our measurements respond to any determinate answer or specifically to deep factual constraints.
3. **Neutral** (NEU,  $n = 52$ ): The distinction between “correct” and “incorrect” tokens does not depend on factual knowledge—for example, completing a syntactically valid but factually unconstrained phrase. If the five measurements defined in Section 3 show no divergence on neutral queries, the phenomena we observe in deep constraint queries cannot be attributed to the forced-completion setup itself.

If the geometric phenomena we measure are specific to factual processing, they should be strongest in DC queries, attenuated in CTRL, and absent in NEU.

Queries span three professional domains—transport regulation ( $n = 100$ ), medical protocols ( $n = 100$ ), and financial compliance ( $n = 100$ )—yielding 300 total queries. Each query specifies a single correct token and a single incorrect token as forced answers, along with manually annotated *deep keywords* (tokens encoding the factual constraint, e.g., “US”, “warfarin”) and surface keywords (tokens providing context without factual specificity, e.g., “ambulance”, “medication”). These annotations are used for attention allocation analysis (M5).

## 4.2 Models

We evaluate four decoder-only transformer models spanning an order of magnitude in parameter count (Table 1). Qwen2 1.5B is the smallest model in our set. We include it to test whether the phenomena we observe require a minimum scale to appear. All models are loaded in `float16` precision with `device_map="auto"` using HuggingFace Transformers [Wolf et al., 2020]. We use eager attention computation (`attn_implementation="eager"`) rather than Flash Attention to obtain explicit per-head attention weight matrices.

## 4.3 Hidden State Extraction

For each of the 300 queries and each model, we run three forward passes: one with the query alone (obtaining  $h_\ell^q$ ), one with the correct token appended (obtaining  $h_\ell^+$ ), and one with the incorrect token appended (obtaining  $h_\ell^-$ ). Hidden states are collected by passing `output_hidden_states=True` as a per-call argument to the model’s forward method.

At each layer  $\ell \in \{0, \dots, L\}$  (where  $\ell = 0$  is the embedding layer output), we extract the residual stream representation at the last token position in the sequence. All hidden states are cast from

Table 1: Models evaluated. All are decoder-only transformers with pre-norm architecture.

Model	Parameters	Layers	$d$	Reference
LLaMA-2 13B	13B	40	5120	[Touvron et al., 2023]
Mistral 7B v0.3	7B	32	4096	[Jiang et al., 2023]
StableLM-2 1.6B	1.6B	24	2048	[Bellagente et al., 2024]
Qwen2 1.5B	1.5B	28	1536	[Yang et al., 2024]

`float16` to `float32` before computing cosine similarities, norms, and displacement vectors, to avoid numerical instability in angular measurements.

For commitment ratio computation (M4), we apply the model’s final layer normalization (`RMSNorm` for LLaMA-2, Mistral, and Qwen2; `LayerNorm` for StableLM-2) to each layer’s hidden state before projecting through the unembedding matrix (`lm_head`). This follows the normalized logit lens variant rather than the raw logit lens of nostalgebraist [2020]. Applying the final normalization stabilizes the projection at early layers where hidden state magnitudes differ substantially from the final layer. The embedding layer ( $\ell = 0$ ) is projected without normalization, as it has not passed through any transformer block.

For attention allocation (M5), we extract attention weight matrices from all heads at each layer via `output_attentions=True`. We measure attention from the last token position to each keyword span, then average across heads within each layer to obtain  $a_\ell(t)$ .

**Token-span matching.** BPE tokenization splits many keywords into multiple sub-word tokens (e.g., “warfarin”  $\rightarrow$  [“war”, “far”, “in”]). We handle this by matching keywords to their character offset spans in the tokenized sequence. We locate each keyword in the original text string, then identify all token positions whose character spans overlap with the keyword. When character offset matching fails, we fall back to token ID subsequence matching. Attention weights are summed across all token positions in a keyword’s span. This approach avoids the systematic underestimation of attention to multi-token keywords that would result from single-token matching.

#### 4.4 Implementation

Linear probes (M3) are L2-regularized logistic regression classifiers implemented in scikit-learn [Pedregosa et al., 2011] with params `C=1.0`, `l1_ratio=0`, `solver='lbfgs'`, and `max_iter=500`.

Probes are trained independently at each layer on the full  $d$ -dimensional hidden states without dimensionality reduction, using 5-fold stratified cross-validation. Input features are the hidden states at the last token position for both correct and incorrect answers concatenated, yielding  $2 \times 300 = 600$  examples per layer.

All code is implemented in PyTorch [Paszke et al., 2019] and HuggingFace Transformers [Wolf et al., 2020], with `scipy` [Virtanen et al., 2020] for statistical tests. All the experiments run on Google Colab using a single NVIDIA Tesla A100 GPU (40GB of VRAM).

#### 4.5 Statistical Analysis

All pairwise comparisons (deep constraint vs. neutral, correct vs. incorrect, within-domain vs. cross-domain) use the Mann-Whitney  $U$  test, chosen because it makes no distributional assumptions on the measurement values. We apply Benjamini-Hochberg false discovery rate (FDR) correction [Benjamini and Hochberg, 1995] across layers within each comparison to control for multiple testing—for

a 40-layer model, each comparison involves 41 simultaneous tests. We report effect sizes as rank-biserial correlation  $r = Z/\sqrt{n}$ , where  $Z$  is the standard normal deviate corresponding to the  $U$ -test  $p$ -value and  $n$  is the total sample size.

Probe accuracy (M3) is reported as mean  $\pm$  standard deviation across 5 folds. Following Hewitt and Liang [2019], we assess probe selectivity by comparing accuracy on deep-constraint queries against neutral-category queries: a probe that performs well on both is detecting forced-completion artifacts, not factual processing.

## 5 Results

### 5.1 Rotational Divergence As Primary Mechanism

When a model processes a correct versus incorrect answer, the internal representations diverge. The question is *how* they diverge. Two possibilities exist. The model could scale the representations—making one pathway “louder” than the other, producing displacement vectors of different lengths. Or it could rotate them—keeping the same magnitude but pointing in different directions, like two arrows of equal length separating on a sphere. These are distinct mechanisms with distinct implications: scaling would mean the model encodes factual correctness as signal strength, while rotation would mean it encodes correctness as position in a geometric space. Our experiments show rotation, not scaling.

Figure 1 shows trajectory similarity  $\tau(\ell)$  across normalized depth for three models (all Qwen2 1.5B values exceed 0.99, consistent with the scale threshold). In LLaMA-2 13B,  $\tau(\ell)$  drops from 0.99 at the embedding layer to a minimum of 0.49 at  $\ell/L = 0.35$  before reconverging to 0.94 at the final layer. Mistral 7B shows a similar pattern ( $\tau_{\min} = 0.51$  at  $\ell/L = 0.31$ ), and StableLM-2 a shallower version ( $\tau_{\min} = 0.79$  at  $\ell/L = 0.42$ ). The divergence is maximal in the middle layers—the model categorizes correct from incorrect answers most strongly at intermediate depth, not at the output.

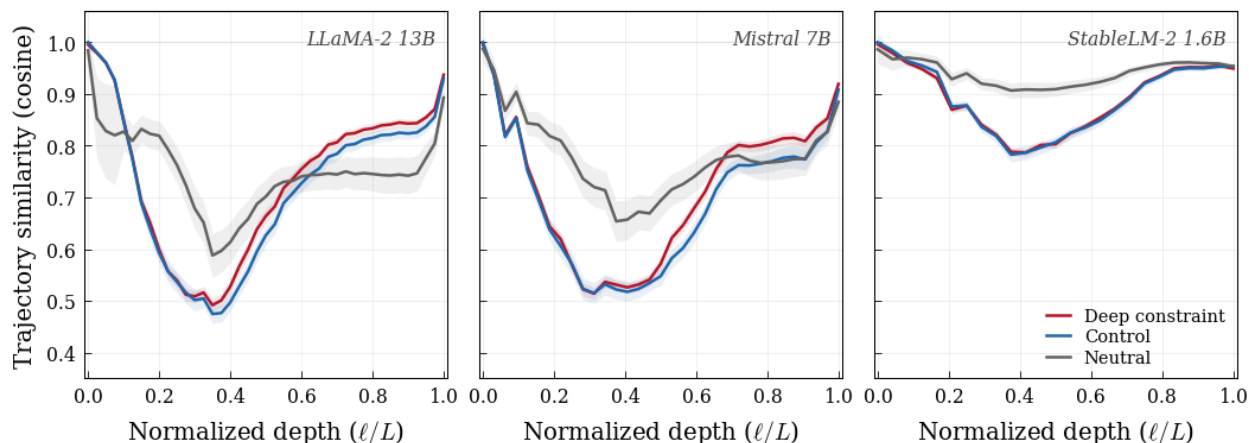


Figure 1: Trajectory similarity  $\tau(\ell)$  between correct and incorrect answer hidden states across normalized depth. Deep constraint (red) and control (blue) queries diverge maximally at  $\ell/L \approx 0.3$ – $0.4$ ; neutral queries (gray) show less divergence. The pattern is absent in Qwen2 1.5B (not shown;  $\tau > 0.99$  at all layers). Shaded regions:  $\pm 1$  SEM.

Two features of this divergence matter for interpretation. First, deep constraint and control categories show nearly identical profiles ( $\tau_{\min} = 0.49$  vs.  $0.47$  in LLaMA-2; not significantly different,

$p_{\text{FDR}} = 0.17$ ), while neutral queries diverge less ( $\tau_{\text{min}} = 0.59$ ; deep vs. neutral:  $r = 0.20$ ,  $p_{\text{FDR}} = 0.010$ , Mann-Whitney  $U$ , FDR-corrected across 41 layers). This means the divergence responds to factual constraint, not to the forced-completion procedure itself.

Second, the divergence is isometric. Table 2 decomposes the divergence into angular and radial components. Across all models and layer depths, the norm ratio  $\eta(\ell)$  stays within 3% of unity (range: 0.97–1.02). The displacement vectors for correct and incorrect answers have the same length. What changes is their direction: the cosine similarity drops to 0.65–0.69 at  $\ell/L = 0.5$  in the two larger models. The model does not distinguish right from wrong by making one signal stronger. It identifies them by pointing the representations in different directions on an approximate hypersphere.

Table 2: Displacement geometry at selected normalized depths. The norm ratio  $\eta$  remains near unity while cosine similarity drops, confirming isometric (rotational) divergence. Values are means across 300 queries per model.

$\ell/L$	LLaMA-2 13B		Mistral 7B		StableLM-2 1.6B	
	$\cos(d^+, d^-)$	$\eta$	$\cos(d^+, d^-)$	$\eta$	$\cos(d^+, d^-)$	$\eta$
0.00	1.00	1.00	1.00	1.00	1.00	1.00
0.10	0.86	1.00	0.87	1.00	0.93	1.00
0.20	0.76	0.99	0.74	1.00	0.86	0.99
0.35	0.68	0.98	0.67	1.00	0.80	1.00
0.50	0.69	0.99	0.65	1.00	0.77	1.00
0.70	0.72	0.99	0.68	1.01	0.81	1.01
1.00	0.78	0.97	0.73	1.01	0.84	0.99

## 5.2 Active Suppression in Incorrect Answers

Figure 2 shows commitment ratio  $\kappa(\ell)$  across depth. For correct answers (solid lines),  $\kappa$  increases monotonically from 0.50 at  $\ell/L = 0$  to 0.77–0.90 at  $\ell/L \approx 0.8$ , with deep constraint queries committing earlier than neutral ones. The striking finding concerns incorrect answers (dashed gray):  $\kappa$  does not only stagnate—it collapses *below* 0.5, reaching  $\kappa_{\text{min}} = 0.08$  in LLaMA-2 (at  $\ell/L = 0.85$ ) and  $\kappa_{\text{min}} = 0.08$  in Mistral 7B (at  $\ell/L = 0.91$ ). StableLM-2 shows a weaker effect ( $\kappa_{\text{min}} = 0.32$  at  $\ell/L = 0.88$ ).

Table 3: Commitment dynamics. For correct answers ( $\kappa_{\text{final}}^+$ ), commitment rises monotonically. For incorrect answers,  $\kappa_{\text{min}}^-$  falls far below 0.5, indicating active suppression. The suppression depth  $\sigma = 0.5 - \kappa_{\text{min}}^-$  quantifies this effect. All  $\kappa_{\text{min}}^-$  values significantly below 0.5 (one-sample  $t$ -test,  $n = 300$ ).

Model	$\kappa_{\text{final}}^+$	$\kappa_{\text{min}}^-$	$\ell^*/L$	$\sigma$	$t$ -statistic	$p$ -value
LLaMA-2 13B	0.77	0.08	0.85	0.42	−36.5	$< 10^{-100}$
Mistral 7B	0.76	0.08	0.91	0.42	−39.1	$< 10^{-100}$
StableLM-2	0.72	0.32	0.88	0.18	−7.9	$< 10^{-13}$
Qwen2 1.5B	0.50	0.50	—	0.00	−0.01	0.99

A model that only failed to engage with the factual constraint would show  $\kappa \approx 0.5$  throughout—the model would be indifferent between the two tokens. This is exactly what Qwen2 1.5B does.

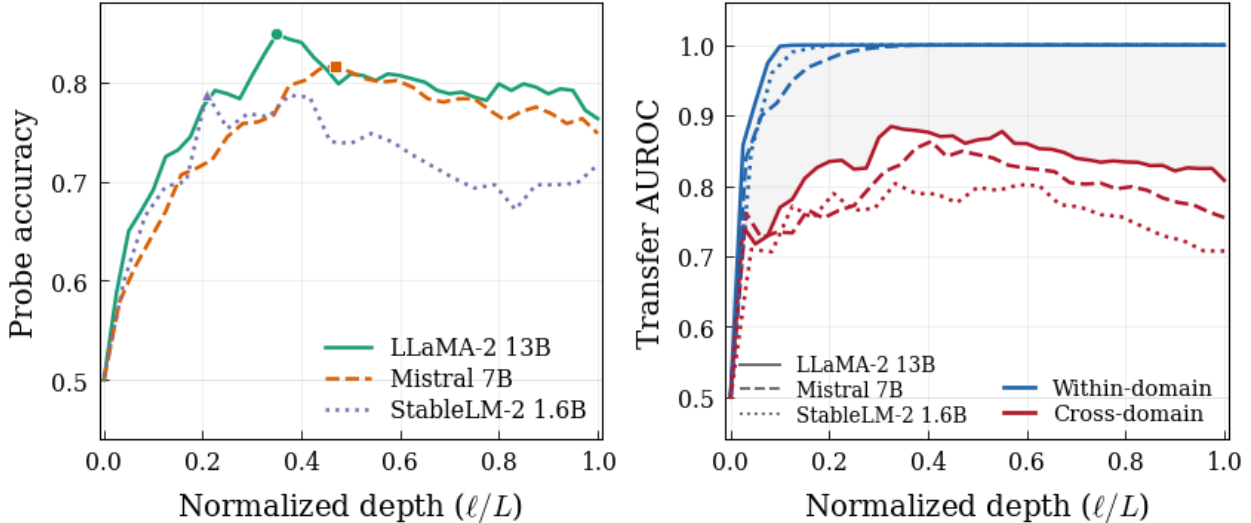


Figure 2: Commitment ratio  $\kappa(\ell)$  across normalized depth. Solid lines: correct answers by category type. Dashed gray: incorrect answers (all categories pooled). In LLaMA-2 and Mistral,  $\kappa$  for incorrect answers collapses below 0.10, indicating active suppression. StableLM-2 shows a weaker effect; Qwen2 1.5B (not shown) remains at 0.50 throughout.

The larger models do something qualitatively different: they drive  $\kappa$  to 0.08, assigning 92% of the intermediate probability mass to the incorrect token.

This suggests a conflict-resolution mechanism rather than passive failure. At intermediate layers, the model retrieves the correct factual association (evidenced by the probing results in Section 5.4). But the residual stream already carries the forced incorrect token. The suppression we observe is consistent with the model computing the discrepancy between retrieved knowledge and actual input—a prediction error that manifests as active rejection of the correct token. The suppression depth scales with model size ( $\sigma$ : 0.42 at 13B, 0.42 at 7B, 0.18 at 1.6B, 0.00 at 1.5B), consistent with stronger factual recall producing larger conflict signals. Establishing the causal role of specific components in this process—particularly mid-layer MLP modules implicated in factual storage [Meng et al., 2022], though recent work has questioned whether causal tracing reliably identifies where knowledge is stored [Hase et al., 2024]—is a natural direction for future work.

The residual stream architecture [Elhage et al., 2021] provides a natural substrate for such conflict: different components write updates into the same shared state, and the suppression we observe is consistent with factual recall modules and input processing producing opposing contributions.

### 5.3 Attention Reallocation Accompanies Suppression

Correct answers consistently allocate more attention to deep-constraint tokens than incorrect answers. Across all layers, mean attention ratios for deep-constraint queries are: LLaMA-2  $\alpha^+ = 0.62$  vs.  $\alpha^- = 0.46$ ; Mistral  $\alpha^+ = 0.60$  vs.  $\alpha^- = 0.42$ ; StableLM-2  $\alpha^+ = 0.61$  vs.  $\alpha^- = 0.42$ . All differences are highly significant (Mann-Whitney  $U$ ,  $p_{\text{FDR}} < 10^{-5}$ , corrected across layers; effect size  $r = 0.24$ – $0.35$ ). This supports that the model’s failure to attend to constraint-bearing tokens is a mechanistic correlate of commitment collapse.

Table 4: Attention allocation to deep-constraint tokens. For queries requiring factual constraints, correct answers attend more to constraint-bearing tokens. FDR correction across all layers per model; effect size  $r$  from Mann-Whitney  $U$ .

Model	$\bar{\alpha}^+$ (correct)	$\bar{\alpha}^-$ (incorrect)	Sig. layers	Max $r$	Best $p_{\text{FDR}}$
LLaMA-2 13B	0.62	0.46	39/41	0.35	$< 10^{-5}$
Mistral 7B	0.60	0.42	31/33	0.35	$< 10^{-5}$
StableLM-2	0.61	0.42	18/25	0.40	$< 10^{-6}$
Qwen2 1.5B	0.48	0.34	0/29	0.07	0.20

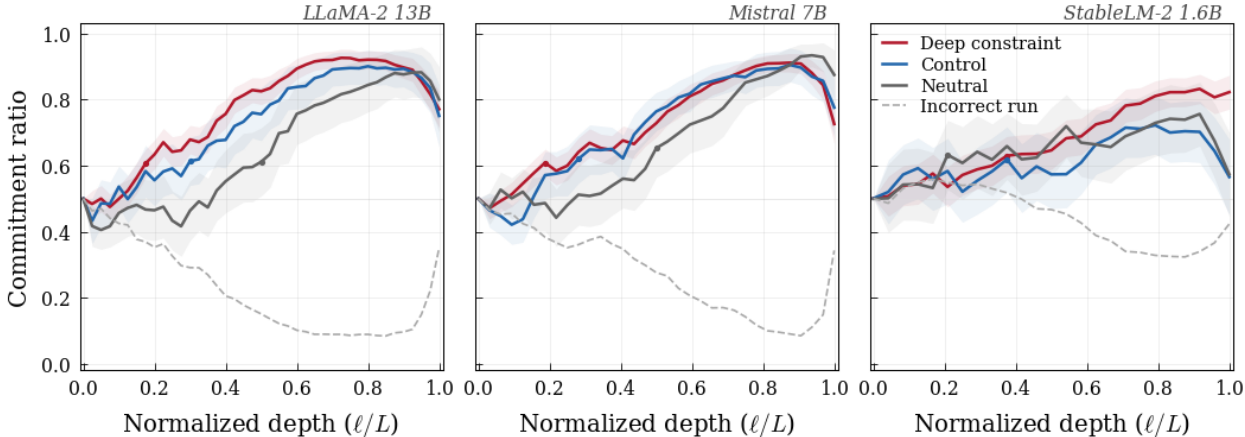


Figure 3: **Left:** Probe accuracy (5-fold CV) across normalized depth. All three models peak at intermediate layers, with accuracy declining toward the final layer. Circles mark peaks. **Right:** Cross-domain transfer AUROC. Within-domain (blue) is near-perfect; cross-domain (red) degrades, particularly for StableLM-2. Qwen2 1.5B (not shown) achieves 0.50 throughout.

#### 5.4 Scale Threshold and Linear Probing

Figure 3 (left panel) shows probe accuracy across depth for three models (Qwen2 achieves only 0.50 at its single valid layer). All three models show peak accuracy at intermediate layers: LLaMA-2 reaches  $0.85 \pm 0.08$  at  $\ell/L = 0.35$ , Mistral  $0.82 \pm 0.09$  at  $\ell/L = 0.47$ , StableLM-2  $0.79 \pm 0.05$  at  $\ell/L = 0.21$ . In all cases, accuracy declines toward the final layer (LLaMA-2: 0.76; Mistral: 0.75; StableLM-2: 0.72). This dissociation between peak probe accuracy and final-layer accuracy is consistent across models ( $\Delta = 0.07\text{--}0.09$ ), though individually the peak-to-final differences reach only marginal significance under a Welch  $t$ -test approximation ( $p \approx 0.10\text{--}0.12$ ; we note this is likely underpowered given 5-fold CV). The pattern suggests that intermediate layers encode factual distinctions more cleanly than the final representation, which must integrate multiple output objectives.

Figure 3 (right panel) shows cross-domain transfer AUROC at  $\ell/L = 0.5$ . Within-domain transfer is near-perfect (mean AUROC = 1.00 for all three models). Cross-domain transfer degrades substantially: LLaMA-2 mean = 0.87 (range 0.78–0.96), Mistral mean = 0.84 (range 0.65–0.99), StableLM-2 mean = 0.80 (range 0.69–0.93). We note that with only three domains, these transfer matrices should be interpreted cautiously; the degradation is consistent with domain-specific encoding but our sample is insufficient to characterize its structure precisely.

Qwen2 1.5B shows no measurable factual processing across any of our five measurements: trajectory similarity  $> 0.99$  at all layers, probe accuracy = 0.50, commitment ratio = 0.50 for both

correct and incorrect answers, attention ratio differences non-significant ( $p_{\text{FDR}} > 0.20$  at all layers), and divergence occurring only at the final layer ( $\ell/L = 0.99$ ). This is evidence of a genuine absence of the computational mechanisms we measure. Combined with the graded pattern across StableLM-2 (1.6B), Mistral (7B), and LLaMA-2 (13B), this suggests a threshold below which transformer models do not develop the internal circuitry for factual constraint processing. Whether this reflects a sharp phase transition [Wei et al., 2022] or a measurement threshold artifact [Schaeffer et al., 2023] cannot be determined from four models alone.

## 6 Discussion

### 6.1 The geometry of factual processing

Our central finding—*isometric divergence*—has a clear implication: methods that detect hallucinations by comparing embedding magnitudes or norms will miss the signal. The discriminative information lives entirely in angular position. This is consistent with the observation that cosine similarity is the dominant metric in embedding-space evaluations, and provides a geometric explanation for why: factual processing naturally produces angular, not radial, separation. We note that contextual representations are highly anisotropic [Ethayarajh, 2019]; our *isometric divergence* claim concerns the displacement vectors  $d_{\ell}^{\pm}$ , not the ambient distribution of hidden states. The rotation we measure occurs within whatever subspace the representations occupy, and holds regardless of the overall anisotropy of the embedding geometry.

The correlation between probe accuracy and commitment gap is positive and significant in LLaMA-2 ( $r = 0.64$ ,  $p < 10^{-5}$ , Pearson) but absent in StableLM-2 ( $r = -0.01$ ,  $p = 0.97$ ). This suggests that in larger models, the layers where factual knowledge is most linearly separable are also those where the model is most actively committing to an answer—a tight coupling between representation and generation that may emerge with scale.

### 6.2 Active suppression as a computational strategy

The collapse of  $\kappa$  to 0.08 is not a necessary consequence of processing incorrect input. A model could process an incorrect answer while remaining agnostic about correctness (maintaining  $\kappa \approx 0.5$ ), as Qwen2 does. Instead, the larger models actively shift their internal representations to *favor* the token they are currently processing—even when that token is factually wrong. This resembles a confirmation bias in the processing pipeline: once the incorrect token enters, the model reinforces it. The suppression depth  $\sigma$  scaling with model size (0.00  $\rightarrow$  0.18  $\rightarrow$  0.42  $\rightarrow$  0.42) suggests that larger models develop stronger internal consistency mechanisms that, as a side effect, more aggressively suppress alternatives.

### 6.3 Implications for hallucination detection

The rotational signature and commitment dynamics we characterize are, in principle, measurable without access to ground-truth labels: we need only the displacement geometry between query and response representations. However, our experimental design uses forced answers with known correct/incorrect tokens, which does not directly apply to open-ended generation where the set of possible answers is wider. Bridging this gap—from controlled forced-completion probing to detection in autoregressive generation—is a necessary next step that we do not attempt here.

## 7 Limitations

Several limitations constrain the generality of our findings:

1. **Dataset scale.** 300 queries across three domains is sufficient for the large effect sizes we observe ( $\sigma = 0.42$ ,  $p < 10^{-100}$ ) but limits our ability to characterize domain-specific structure. The cross-domain transfer analysis involves only a  $3 \times 3$  matrix per model.
2. **Forced answer vs. autoregressive generation.** Our method appends a single token and observes the resulting hidden states. In natural generation, the model autoregressively selects tokens, and the dynamics of this selection process may differ from forced processing. Our results characterize how models process correct vs. incorrect continuations, not how they choose between them.
3. **Architecture scope.** All four models are decoder-only transformers. Encoder-decoder models may show different dynamics, and we have not studied models with retrieval augmentation.
4. **Probe dissociation significance.** The peak-to-final accuracy gap ( $\Delta = 0.07$ – $0.09$ ) is consistent across models but individually reaches only  $p \approx 0.10$ – $0.12$ . This is likely underpowered with 5-fold CV; we report the pattern without claiming statistical significance for individual models.
5. **Qwen2 architecture.** The lack of measurable phenomena in Qwen2 1.5B could reflect architectural differences rather than scale alone. We cannot fully disentangle model family from parameter count with only four models.

## 8 Conclusions

This paper establishes a specific geometric fact about transformer internals: when these models process factual queries, they characterize correct and incorrect answers through rotation in representation space, not through scaling. The displacement vectors for both types of answers have the same magnitude. What differs is their direction. We have directly measured this property in the hidden-state geometry, confirmed across three model scales.

The active suppression result adds a mechanistic dimension. Transformers do not passively fail to retrieve facts when processing incorrect input. They retrieve the correct association and then actively drive the representation away from it. This behavior is consistent with a conflict-resolution process between retrieved knowledge and observed input. This is not observed in models below 1.6B parameters and strengthens with scale, suggesting that it’s a property of how factual processing emerges rather than how it’s encoded.

Two limitations bound these conclusions. First, forced-completion probing controls for confounds by constraining the experimental setup to single-token continuations. Whether the rotational geometry persists in free-form autoregressive generation—where the model selects its own tokens—remains untested. Second, four models cannot characterize a phase transition. The 1.5B/1.6B boundary is suggestive, but establishing whether the threshold is sharp or gradual requires systematic evaluation across dozens of model scales.

The broader question is whether the rotational geometry we observe is specific to factual processing or is a general mechanism by which transformers represent categorical distinctions in the residual stream. If rotational divergence turns out to be how these architectures encode any binary semantic distinction—not just factual correctness—that would be a finding about transformer

computation itself, not just about hallucination. Conversely, if it’s specific to factual constraints, it provides a geometric target for detection methods that do not rely on another model’s judgment. Either answer advances understanding of what these systems actually compute.

## References

- Amos Azaria and Tom Mitchell. The internal state of an LLM knows when it’s lying. In *Findings of the Association for Computational Linguistics: EMNLP*, 2023.
- Marco Bellagente, Jonathan Tow, Dakota Mahan, Duy Phung, Maksym Zhuravynskyi, Reshynth Adithyan Sauer, et al. Stable LM 2 1.6B technical report. *arXiv preprint arXiv:2402.17834*, 2024.
- Nora Belrose, Zach Furman, Logan Smith, Danny Halawi, Igor Ostrovsky, Lev McKinney, Stella Biderman, and Jacob Steinhardt. Eliciting latent predictions from transformers with the tuned lens. In *Advances in Neural Information Processing Systems*, volume 36, 2023.
- Yoav Benjamini and Yosef Hochberg. Controlling the false discovery rate: A practical and powerful approach to multiple testing. *Journal of the Royal Statistical Society: Series B*, 57(1):289–300, 1995.
- Collin Burns, Haotian Ye, Dan Klein, and Jacob Steinhardt. Discovering latent knowledge in language models without supervision. In *International Conference on Learning Representations*, 2023.
- Damai Dai, Li Dong, Yaru Hao, Zhifang Sui, Baobao Chang, and Furu Wei. Knowledge neurons in pretrained transformers. In *Proceedings of the 60th Annual Meeting of the Association for Computational Linguistics (Volume 1: Long Papers)*, pages 8493–8502, 2022.
- Guy Dar, Mor Geva, Ankit Gupta, and Jonathan Berant. Analyzing transformers in embedding space. In *Proceedings of the 61st Annual Meeting of the Association for Computational Linguistics*, 2023.
- Alexander Yom Din, Noga Tamir, Idan Szpektor, and Yoav Goldberg. Jump to conclusions: Short-cutting transformers with linear transformations. *arXiv preprint arXiv:2303.09435*, 2023.
- Nelson Elhage, Neel Nanda, Catherine Olsson, Tom Henighan, Nicholas Joseph, Ben Mann, Amanda Askell, Yuntao Bai, Anna Chen, Tom Conerly, et al. A mathematical framework for transformer circuits. *Transformer Circuits Thread*, 2021.
- Kawin Ethayarajh. How contextual are contextualized word representations? comparing the geometry of BERT, ELMo, and GPT-2 representations. In *Proceedings of the 2019 Conference on Empirical Methods in Natural Language Processing*, 2019.
- Mor Geva, Roei Schuster, Jonathan Berant, and Omer Levy. Transformer feed-forward layers are key-value memories. In *Proceedings of the 2021 Conference on Empirical Methods in Natural Language Processing*, 2021.
- Mor Geva, Jasmijn Bastings, Katja Filippova, and Amir Globerson. Dissecting recall of factual associations in auto-regressive language models. In *Proceedings of the 2023 Conference on Empirical Methods in Natural Language Processing*, 2023.

- Wes Gurnee and Max Tegmark. Language models represent space and time. In *International Conference on Learning Representations*, 2024.
- Peter Hase, Mohit Bansal, Been Kim, and Asma Ghandeharioun. Does localization inform editing? surprising differences in causality-based localization vs. knowledge editing in language models. In *Advances in Neural Information Processing Systems*, volume 37, 2024.
- Evan Hernandez, Arnab Sen Sharma, Tal Haklay, Kevin Meng, Martin Wattenberg, Jacob Andreas, Yonatan Belinkov, and David Bau. Linearity of relation decoding in transformer language models. In *International Conference on Learning Representations*, 2024.
- John Hewitt and Percy Liang. Designing and interpreting probes with control tasks. In *Proceedings of the 2019 Conference on Empirical Methods in Natural Language Processing*, 2019.
- Lei Huang, Weijiang Yu, Weitao Ma, Weihong Zhong, Zhangyin Feng, Haotian Wang, Qianglong Chen, Weihua Peng, Xiaocheng Feng, Bing Qin, et al. A survey on hallucination in large language models: Principles, taxonomy, challenges, and open questions. *arXiv preprint arXiv:2311.05232*, 2023.
- Ziwei Ji, Nayeon Lee, Rita Frieske, Tiezheng Yu, Dan Su, Yan Xu, Etsuko Ishii, Ye Jin Bang, Andrea Madotto, and Pascale Fung. Survey of hallucination in natural language generation. *ACM Computing Surveys*, 55(12):1–38, 2023.
- Albert Q Jiang, Alexandre Sablayrolles, Arthur Mensch, Chris Bamford, Devendra Singh Chaplot, Diego de las Casas, Florian Bressand, Gianna Lengyel, Guillaume Lample, Lucile Saulnier, et al. Mistral 7B. *arXiv preprint arXiv:2310.06825*, 2023.
- Kenneth Li, Oam Patel, Fernanda Viégas, Hanspeter Pfister, and Martin Wattenberg. Inference-time intervention: Eliciting truthful answers from a language model. In *Advances in Neural Information Processing Systems*, volume 36, 2023.
- Samuel Marks and Max Tegmark. The geometry of truth: Emergent linear structure in large language model representations of true/false datasets. *arXiv preprint arXiv:2310.06824*, 2023.
- Kevin Meng, David Bau, Alex Andonian, and Yonatan Belinkov. Locating and editing factual associations in GPT. In *Advances in Neural Information Processing Systems*, volume 35, 2022.
- nostalgebraist. interpreting GPT: the logit lens. *LessWrong*, 2020.
- Kiho Park, Yo Joong Choe, and Victor Veitch. The linear representation hypothesis and the geometry of large language models. In *International Conference on Machine Learning*, 2024.
- Adam Paszke, Sam Gross, Francisco Massa, Adam Lerer, James Bradbury, Gregory Chanan, Trevor Killeen, Zeming Lin, Natalia Gimelshein, Luca Antiga, et al. Pytorch: An imperative style, high-performance deep learning library. In *Advances in Neural Information Processing Systems*, volume 32, 2019.
- Fabian Pedregosa, Gaël Varoquaux, Alexandre Gramfort, Vincent Michel, Bertrand Thirion, Olivier Grisel, Mathieu Blondel, Peter Prettenhofer, Ron Weiss, Vincent Dubourg, et al. Scikit-learn: Machine learning in python. *Journal of Machine Learning Research*, 12:2825–2830, 2011.
- Rylan Schaeffer, Brando Miranda, and Sanmi Koyejo. Are emergent abilities of large language models a mirage? In *Advances in Neural Information Processing Systems*, volume 36, 2023.

- Hugo Touvron, Thibaut Lavril, Gautier Izacard, Xavier Martinet, Marie-Anne Lachaux, Timothée Lacroix, Baptiste Rozière, Naman Goyal, Eric Hambro, Faisal Azhar, et al. LLaMA: Open and efficient foundation language models. *arXiv preprint arXiv:2302.13971*, 2023.
- Pauli Virtanen, Ralf Gommers, Travis E Oliphant, Matt Haberland, Tyler Reddy, David Cournapeau, Evgeni Burovski, Pearu Peterson, Warren Weckesser, Jonathan Bright, et al. Scipy 1.0: Fundamental algorithms for scientific computing in python. *Nature Methods*, 17:261–272, 2020.
- Jason Wei, Yi Tay, Rishi Bommasani, Colin Raffel, Barret Zoph, Sebastian Borgeaud, Dani Yogatama, Maarten Bosma, Denny Zhou, Donald Metzler, et al. Emergent abilities of large language models. *Transactions on Machine Learning Research*, 2022.
- Thomas Wolf, Lysandre Debut, Victor Sanh, Julien Chaumond, Clement Delangue, Anthony Moi, Pierric Cistac, Tim Rault, Remi Louf, Morgan Funtowicz, et al. Transformers: State-of-the-art natural language processing. In *Proceedings of the 2020 Conference on Empirical Methods in Natural Language Processing: System Demonstrations*, pages 38–45, 2020.
- An Yang, Baosong Yang, Binyuan Hui, Bo Zheng, Bowen Yu, Chang Zhou, et al. Qwen2 technical report. *arXiv preprint arXiv:2407.10671*, 2024.
- Andy Zou, Long Phan, Sarah Chen, James Campbell, Phillip Guo, Richard Ren, Alexander Pan, Xuwang Yin, Mantas Mazeika, Ann-Kathrin Dombrowski, et al. Representation engineering: A top-down approach to AI transparency. *arXiv preprint arXiv:2310.01405*, 2023.